BNL-95158-2011-JA

PROGRESS IN PHOTOVOLTAICS: RESEARCH AND APPLICATIONS
Prog. Photovolt: Res. Appl. 2011; **19**:228–239
Published online 15 July 2010 in Wiley Online Library (wileyonlinelibrary.com). DOI: 10.1002/pip.990

BROADER PERSPECTIVES

Comparative life-cycle energy payback analysis of multi-junction a-SiGe and nanocrystalline/a-Si modules

H.C. Kim[1] and V.M. Fthenakis[1,2]*

[1] Center for Life Cycle Analysis, Columbia University, NY, USA
[2] Photovoltaic Environmental Research Center, Brookhaven National Laboratory, Upton, NY, USA

ABSTRACT

Despite the publicity of nanotechnologies in high tech industries including the photovoltaic sector, their life-cycle energy use and related environmental impacts are understood only to a limited degree as their production is mostly immature. We investigated the life-cycle energy implications of amorphous silicon (a-Si) PV designs using a nanocrystalline silicon (nc-Si) bottom layer in the context of a comparative, prospective life-cycle analysis framework. Three R&D options using nc-Si bottom layer were evaluated and compared to the current triple-junction a-Si design, i.e., a-Si/a-SiGe/a-SiGe. The life-cycle energy demand to deposit nc-Si was estimated from parametric analyses of film thickness, deposition rate, precursor gas usage, and power for generating gas plasma. We found that extended deposition time and increased gas usages associated to the relatively high thickness of nc-Si lead to a larger primary energy demand for the nc-Si bottom layer designs, than the current triple-junction a-Si. Assuming an 8% conversion efficiency, the energy payback time of those R&D designs will be 0.7–0.9 years, close to that of currently commercial triple-junction a-Si design, 0.8 years. Future scenario analyses show that if nc-Si film is deposited at a higher rate (i.e., 2–3 nm/s), and at the same time the conversion efficiency reaches 10%, the energy-payback time could drop by 30%. Copyright © 2010 John Wiley & Sons, Ltd.

KEYWORDS
nano, life-cycle analysis, primary energy, energy payback time, amorphous silicon

***Correspondence**
V.M. Fthenakis, Photovoltaic Environmental Research Center, Brookhaven National Laboratory, Upton, NY, USA.
E-mail: vmf@bnl.gov

Received 11 August 2009; Revised 17 January 2010

1. INTRODUCTION

Increasing attention to the potential effects of nanotechnology on human- and ecological-health triggered the recent surge of life-cycle analysis (LCA) studies of, for example, carbon nanofibres (CNFs), polymer nanocomposites, nanoscale platinum-group metal (PGM) particles, nanoscale semiconductors, and nanoparticle titania [1–8]. Producing nanostructures tends to be more energy intensive per unit mass than fabricating conventional structures. For instance, from cradle-to-grave, CNFs require 13–50 times more primary energy per mass basis than does primary aluminum [2]. Synthesizing nanoparticle titania requires further milling and surface treatment after completing the classical processes, suggesting an elevated energy requirement for micro-size titania particles [7]. However, if their usage phase is accounted for, the nanoparticle-based composites may achieve a net energy savings over their entire life cycle compared with conventional materials since lesser amounts can be used to meet their materials properties, like stiffness and strength [1,8]. Overall, our current understanding of the energy- and emissions-implications of these products carries a large degree of uncertainty due to the limited data available [6,9]. Considering the complexity of the topic, i.e., the variety of shapes, usages, and production methods, the existing LCA framework and the data-gathering techniques may need to be refined [9]. Notwithstanding, there will be benefits in proactively assessing the potential environmental risks of a nanotechnology before it fully matures [10].

Recent years witnessed a surge of production and installation of photovoltaic (PV) devices, along with increasing worldwide interest in clean, abundant sources of energy. Thin-film amorphous silicon (a-Si) PVs are one of the most promising options, mainly due to their unique

Copyright © 2010 John Wiley & Sons, Ltd.

advantages over bulk crystalline silicon (c-Si) PVs, including low material cost, aesthetic attractiveness, and easy integration into a building. Since the first thin-film a-Si cell with a conversion efficiency of 2.4% was fabricated in 1976, numerous studies entailed improvements in its optical- and electronic-properties [11,12]. Reportedly, the highest confirmed stabilized efficiency for a triple-junction R&D module is 10.4% under the standard test condition (measured under the global AM1.5 spectrum (1000 W/m^2) at a cell temperature of 25°C). As yet, commercial lines produce modules with a 6–7% stabilized total-area efficiency [13–15]. The world production of a-Si modules in 2008 is estimated at 434 MW$_p$, accounting for roughly 40% of the total thin-film production [16]. The future is even brighter, as large thin-film equipment manufacturers, like Oerlikon and Applied Materials, plan to launch or expand the manufacture of a-Si PV lines.

The current a-Si PV modules are less efficient than other major commercial thin-film technologies, like CdTe and CIGS, which convert over 10% of photon energy to electricity. In attempting to increase conversion efficiency, researchers are engineering nanoscale materials that involve a scale of about 100 nm for a-Si device designs. In fact, incorporating nanotechnologies into cell design was actively explored by the PV industrial sector, either to improve existing systems like thin-film CdTe, or develop new systems like dye-sensitized cells. In parallel, revolutionary designs were examined based on novel semiconductor physics, although their commercialization seems distant. Examples of such designs include solar cells using quantum dots and multiple electron-hole pair generation per photon [14,17].

Analyzes have been undertaken on the life cycle of a-Si PVs since the early 1990s [18]. However, only a few studies investigated large-scale, commercial a-Si PV lines [19–21]. Keoleian and Lewis (1997) measured the energy-payback time (EPBT) and life-cycle energy return of United Solar's tandem-junction a-Si module with a 5% stabilized conversion efficiency at multiple locations in the United States [19]. They reported that a frameless a-Si module deposited on a stainless-steel substrate pays back the energy investment used in production after 4.6 years of generating electricity in Detroit, Michigan where insolation is 1200 kWh/m^2/year, and after 2.2 years in Phoenix, Arizona where insolation is 2480 kWh/m^2/year. The warranty lifetime of 10 years for this early module corresponded to an energy return of 2.19 in the former location, and 4.52 in the latter [19]. Later, the same researchers investigated the energy payback and life-cycle emissions of United Solar's triple-junction a-Si module with a 6.3% stabilized conversion efficiency, reporting an EPBT of 3.2 years for a specific rooftop installation tuned for an insolation of 1360 kWh/m^2 [21].

Despite growing concerns about the potential risks to humans and ecosystems, the life-cycle impact of nanotechnology-based PVs are imprecisely understood because data are rare since they are not yet in commercial production [22]. The aim of this study is to investigate the energy implications of nanotechnology-based a-Si PV systems that are currently under R&D. The framework that this study employs, i.e., comparative analyses of micro- and nanotechnology, is described elsewhere [22]. We use an LCA tool to compare the primary energy demand of the current a-Si-based PV module and a future nanostructure-based PV module being developed by United Solar. We formulate the energy requirements during the deposition process based on industrial sources, literature, and commercial- and public-life-cycle databases. A commercialized, nanostructure-based module, i.e., ''Micromorph'', is compared with the aforementioned designs in terms of energy demand during production. We also discuss the industrial policy implications and the uncertainty of the analyses.

2. AMORPHOUS & NANOCRYSTALLINE SILICON-BASED MULTI-JUNCTION PV MODULES

The exciting features of a-Si solar cells have been driving numerous industrial and academic R&D explorations and scaling-up efforts for this type of PV. With its disorderly crystal structure, a-Si has higher optical absorption than does c-Si, thus requiring less material to absorb the desired range of the solar spectrum (c-Si) [11]. Fabricating thin-film a-Si relies on deposition processes that are simple and inexpensive compared to those for bulk c-Si PVs. a-Si films can be deposited on glass as well as on flexible stainless steel substrates resulting in a flexible module perfect for building integrated applications. In addition, a-Si easily alloys with Ge and C during film deposition to adjust the bandgap, and thus is suitable for multi-junction cells in which each layer of thin film coverts a different spectrum of sunlight, e.g., a-Si/a-SiGe/a-SiGe triple junction.

The layout of a-Si cell for a single junction resembles a photodiode consisting of an undoped i-layer, a boron (B) doped p-layer, and a phosphorus (P) doped n-layer. Each doped layer typically is formed by adding phosphine (PH_3)- or diborane (B_2H_6)- gases with other precursor gases. Some manufacturers use boron trifluoride (BF_3) gas for the p-layer. The i-layer is 200–300 nm thick, absorbing most of the spectrum in visible light, with the $\sim$20 nm thick p-and n- layers on each side of the i-layer to build an electric field. An a-Si solar cell generates electricity when the electrons and holes generated by photons are transported, correspondingly, to the n- and p-layers by the built-in electric field.

The typical a-Si cell is alloyed with hydrogen during cell deposition, passivating any broken Si bonds with hydrogen atoms to reduce defects and enhance opto-electronic properties [12]. The hydrogenated amorphous silicon, a-Si:H is grown by the plasma-enhanced chemical vapor deposition (PECVD) technique that normally uses radio frequency oscillations (RF-13.56 MHz) to create a gas plasma from mixture of SiH_4 and H_2 gases. The

microstructure and growth kinetics of a-Si:H film depend on the gas composition and pressure, as well as plasma power density during the deposition. a-Si:H, however, suffers from ''Staebler-Wronski Effect (SWE)'' that significantly degrades the efficiency of the cell upon exposure to sunlight [11,23]. For example, there is a loss of as much as 30% for a single-junction a-Si cell after 1000 h of illumination when it is stabilized [24]. Since a thick intrinsic layer deteriorates deeper than a thinner one, early approaches to abating this effect focused on thinning the intrinsic layer as much as possible with advanced optical reflectors to compensate for the lower absorption of sunlight consequent upon the reduced thickness [12,23]. Increased hydrogen dilution in the precursor gas mixture improves stability, but lowers the deposition rate [25]. Empowered by the a-SiGe-alloy deposition technology, the current commercialized a-Si modules mostly employ multi-bandgap multi-junction approaches to avoid a thick single-junction intrinsic layer, while, at the same time, converting more photons into electricity and limiting degradation to 12–15%. Degradation with nc-Si layers is even less.

Recent developments in mitigating the SWE and increasing conversion efficiency center on hybridizing amorphous- and nanocrystalline-Si (nc-Si) layers as the latter barely suffers from sunlight-induced degradation. An nc-Si film is formed when silicon is deposited from a high H_2-dilution gas mixture with an H_2 dilution ratio $R\,(=[H_2]/[SiH_4])$ of over 10 [26]. PV manufacturers are developing tandem-junction, hybrid amorphous- and crystalline-silicon devices that consist of a high bandgap (~ 1.7 eV) a-Si top cell, and low bandgap (~ 1.1 eV) nc-Si bottom cell [27]. Triple-junction configurations are being explored in attempting to optimize the design. The grain size of nanocrystalline in a nc-Si layer typically is around 50 nm although the layer often conventionally is called 'microcrystalline (μc)' [25,28]. Besides its better stability in sunlight, this design avoids using expensive GeH_4 gas, a precursor of a-SiGe-based multi-junctions.

However, because nc-Si has an indirect bandgap, its absorption coefficient is relatively low for the target solar-spectrum of the bottom layer, i.e., >700 nm. Accordingly, a thick layer, i.e., 1–3 μm of film is required for sufficient light absorption [25,28]. Growing such a thick layer would necessitate a long deposition time, thereby severely limiting the throughput of equipment at the current deposition rate of a-Si cells, 0.1–0.3 nm/s [29]. To increase the deposition rate, an nc-Si thin film typically is grown under the high gas pressure and high plasma power regime of PECVD process [30]. The highest deposition rate is achieved when the PECVD is combined with Very High Frequency (VHF), a plasma excitation frequency of 40–75 MHz rather than 13.56 MHz commonly employed in PECVD. The deposition rate must be accelerated at least to 2–3 nm/s to lay down the nanocrystalline structure in a comparable time to the current deposition cycle of a triple-junction module [11]. In parallel, film thicknesses and material properties must be uniform over a large active area to secure the improved efficiency of this module's design. The deposition rate of nc-Si layer currently remains at 0.5–0.8 nm/s for R&D phase of a-Si:H/nc-Si:H modules. The latest stabilized efficiency of this type measured in a small aperture area is $\sim 12\%$ [13].

3. LCA OF NANOTECHNOLOGY - BASED MULTI-JUNCTION PV

3.1. Scope of analysis

We investigated the life-cycle environmental indicators for nanostructure-based a-Si PV modules, comparing the findings with those from current a-Si PV technologies. For the latter, we modeled a triple-junction a-Si module, a-Si:H/a-SiGe:H/a-SiGe:H, while for nanotechnology-based PVs, we assessed three combinations of hybrid amorphous- and crystalline-silicon cells (Figure 1) being developed by United Solar. The first configuration is a tandem junction that consists of a-Si top layer and nc-Si bottom layer, i.e., a-Si:H/nc-Si:H; the second configuration is a triple junction with nc-Si as the bottom layer, i.e., a-Si:H/a-SiGe:H/nc-Si:H; and, lastly, a triple junction with two layers of nc-Si, i.e., a-Si:H/nc-Si:H/nc-Si:H. Oerlikon Solar developed a design called 'Micromorph' that employs a glass substrate on which it deposited a TCO layer (transparent conductive oxide), followed by a-Si- and nc-Si-films. The life-cycle energy demand of this design will be approximately evaluated later in this paper and compared with the present designs investigated.

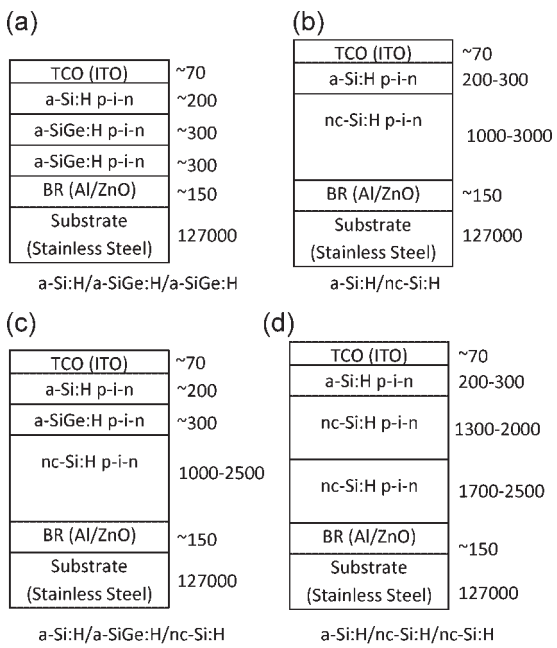

Figure 1. Dimensions, all in nm, of the modeled PV designs [32,35,36,59] (encapsulation is not shown here).

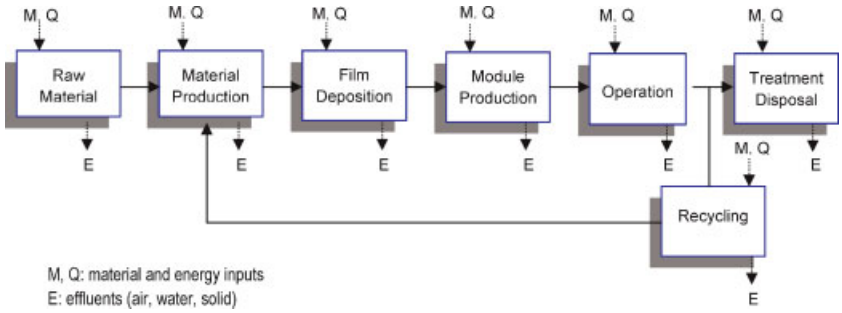

Figure 2. Life cycle of thin-film PV.

The life cycle of a thin-film PV module starts from acquiring and processing materials, then encompasses film deposition, module production and operation, and ends at recycling or disposal (Figure 2). We did not consider recycling or the disposal stage mainly because data are lacking, although a study is underway on the end-of-life options of PV modules [31]. Estimates from LCA databases such as Ecoinvent, Franklin, and IDEMAT and from a report by Pacca *et al*. (2005) [35] were used in evaluating the raw-material acquisition and materials-production stages [32]; the film deposition and production stages where nanotechnologies are implemented were investigated in detail. Electricity generation during the operation phase was modeled in accordance with the recommended parameter values of the International Energy Agency (IEA) [33].

United Solar employs a 'roll-to-roll' PECVD process wherein active layers are deposited in sequence on a flexible stainless-steel substrate as it moves through deposition chambers to guarantee a quality uniform product and save equipment and operational costs [34]. The detailed materials and energy input data for United Solar's triple-junction a-Si, ASR-128, is shown elsewhere [35]. Produced until 2002, this a-Si module has a dimension of 5600 mm × 400 mm and a conversion efficiency of 6.0%. Our analysis of current a-Si design bases PVL-136, one of the currently produced a-Si PV modules. Pacca *et al*. (2007) [21,59] evaluated the life-cycle primary energy of PVL-136 a-Si based on the ASR-128 inventory data along with updated electricity, natural gas, and water consumption data [22,36]. PVL-136 has the same three-layered configuration as ASR-128 and a similar dimension of 5500 mm × 400 mm, but a slightly higher efficiency of 6.3%. Figure 3 breaks down the primary energy requirements from the raw material stage to that of module production stages. Assumptions have been made regarding the primary energy demand of some materials whose data are unavailable. For example, the primary energy embedded per kg in minor precursor gases such as GeH_4 is assumed to be the same as that in silane (SiH_4). Similarly, the primary energy value per kg of phosphine (PH_3) dopant was used for diborane (B_2H_6). Not included was the embedded primary energy of TCO (indium tin oxide) layer, which accounts for less than 0.01% of the total module mass; only energy for sputtering the layer was included. Electricity is the major source of primary energy demand, along with the encapsulation materials, i.e., EVA, HDPE, LDPE, Tefzel, and glass fiber. Although expensive, the precursor gases, i.e., SiH_4 and H_2, and the dopant gases account for only 1% of the total energy requirement.

3.2. Electricity use

For modeling the energy requirement of the nc-Si layer, we estimated the consumption of electricity and fuel per unit thickness of a-Si layer by roll-to-roll deposition in the production of United Solar's PVL-136 module. Figure 3 shows the breakdown of primary energy requirement which is derived from the electricity (primary energy equivalent) and fuel usages. In particular, we used the electric-energy demand and the parameters for PECVD of PVL-136 layers as references to derive the energy demand of other silicon layers. The primary energy consumption during PECVD was modeled as a function of the deposition rate and plasma power based on the SEMATECH's energy-usage data for a 300 mm two-chamber

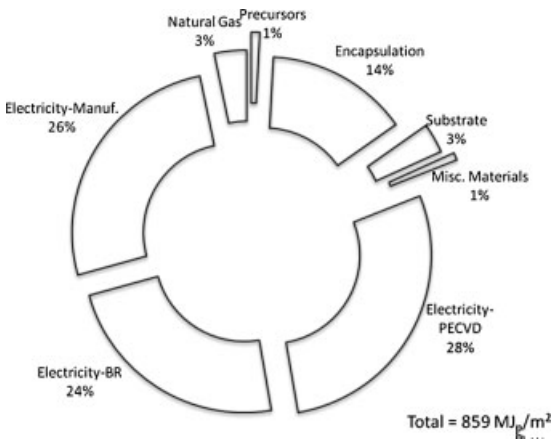

Figure 3. Breakdown of primary energy requirement for a triple junction a-Si/a-SiGe/a-SiGe. BR=back reflector; PECVD=plasma-enhanced chemical vapor deposition [35,59].

Table I. Breakdown (%) of power requirement of PECVD [38].

Component[a]	Reactor 1 (%)	Reactor 2 (%)
	Total = 6.8 kW	Total = 7.5 kW
Heater	14.7	8.0
Vacuum pump	52.9	56.0
Plasma generation	8.8	18.7
RF generation for cleaning[b]	4.4	4.0
Water handling pump	13.2	NA
Miscellaneous	5.9	13.3

[a] Input-output chamber pump, power supply controller, and environment control units are not included.
[b] Dissociate perfluoro-compound (PFC) input gases to clean chamber deposits.
RF = radio frequency; NA = not applicable.

PECVD tool [37,38]. Table I summarizes the electric-power demand of the two PECVD chambers that can operate under multiple loads, depending on the process stage, i.e., idle, low-load, or high-load. Table I lists only high-load operation corresponding to a full-power condition. Since the roll-to-roll process operates at a steady power (kW) with the plasmas, gas flows, and heaters always on to assure uniform quality [34], we modeled the energy requirement during PECVD as proportional to deposition time and film thickness. The electricity for generating plasma for depositing nc-Si film, which accounts for 14% of the total use, was modeled separately (Equations (1)–(3)).

$$E = E_D + E_R \tag{1}$$

$$E_D = a \times \left(\frac{L}{R}\right) \tag{2}$$

$$E_R = \begin{cases} b \times \left(\frac{L}{R}\right) & \text{for a-Si} \\ c \times R^{1.3} \times \left(\frac{L}{R}\right) & \text{for nc-Si} \end{cases} \tag{3}$$

where E_D is electricity demand for the PECVD system (heater, pumps, cleaning, and miscellaneous), E_R is electricity demand for plasma generation, L is layer thickness, R is deposition rate, and a, b, c are constants.

We assume that the deposition rate (R) of the current a-Si film is 0.1–0.3 nm/s, whereas that of nc-Si film is 0.5–0.8 nm/s (Table II) [39], although we note that some manufactures may exceed this rate [32,40]; the latter employs a higher radio frequency and excitation power than the former to boost the deposition rate. We anticipate that in future this value should be 2-3 nm/s for nc-Si film to be competitive with a-Si based PVs (Table II) [39], indicating that the deposition time, and correspondingly, the energy requirement, E_D, will fall dramatically. The reference deposition rate for nc-Si layer is 0.65 and 2.5 nm/s, respectively, for the current and future scenarios. On the other hand, industry's experiences show that the rate of nc-Si film deposition rises with the power density on the electrode [30,41,42]. Its power demand during such deposition is approximated as being proportional to $R^{1.3}$ according to Hamers *et al*. (2007) [41]. This results in the electricity demand for plasma generation, E_R, being correlated to $R^{0.3}$(Equation (3)). Also, we assumed that other changes in parameters, like substrate temperature and gas pressure, during an elevated deposition rate do not affect the electricity demand of deposition. Finally, we considered that the electricity requirement for module manufacturing and back-reflector deposition remains unchanged for nc-Si layer incorporated designs.

3.3. Gas usage

During the deposition of silicon thin film, several operating parameters, including the gas mixture, gas flow-rates, substrate temperature, and RF power contribute to form a spectrum of structure, i.e., from an amorphous- to a crystalline-silicon film. Optimal a-Si is deposited just on the low dilution side of the nc-Si transition, so called ''on-the-edge'' material since density of defects in the film is minimal in this zone, thus realizing the lowest degradation when exposed to light [43]. Diluting the precursor silane gas with hydrogen is the most common technique in growing an nc-Si layer. Figure 4 illustrates this hydrogen-dilution effect on the phase transition [44]. In the low-silane concentration (Regime 1), the nc-Si phase emerges as hydrogen dilution increases; the crystallinity and grain size of nc-Si film increase with increase in H_2 dilution [45]. However, as Figure 4 shows, material utilization and the deposition rate are limited by the low SiH_4 depletion. On the other hand, high-quality nc-Si film also can be deposited under a high-silane concentration regime [44]. Owing to the high-silane depletion during PECVD, material utilization is very high in Regime 2 that is amenable to a high rate nc-Si deposition. The usages of SiH_4 and H_2 during the deposition of nc-Si are unavailable and we estimated them on the basis of the gas-input inventory of United Solar's ASR-128 (Table II) [35]. First,

Table II. Primary modeling parameters for a-Si and nc-Si layers [35,42,44]. Reference estimates are in brackets.

	a-Si, current	a-Si, future	nc-Si, current	nc-Si, future
Deposition rate (nm/s)	0.1–0.3 [0.2]	0.2–0.4 [0.3]	0.5–0.8 [0.65]	2–3 [2.5]
SiH_4 Concentration (%) in H_2	2	2	1	4
SiH_4 utilization (%)	20	20	20	80

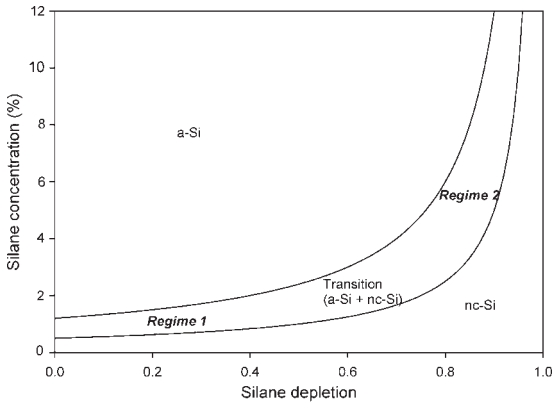

Figure 4. Silane concentration and phase-transition diagram. Silane depletion is defined as the reduction ratio of silane partial pressure due to the dissociation by plasma [44].

we assumed that the mass of silane-gas use per unit nc-Si thickness is the same as that for a-Si considering their similar density [46]. For the current nc-Si with a moderate deposition rate, 0.5–0.8 nm/s, the SiH_4 concentration in a precursor gas mixture is considered to be 1% with a 20% utilization rate, representing Regime 1 in Figure 4. For future nc-Si with a high deposition rate, 2–3 nm/s, we estimate that the concentration will jump to 4% with 80% utilization when the film is grown under Regime 2. Present-day deposition of nc-Si requires twice as much H_2 per unit thickness as that for depositing a-Si, whilst the use of SiH_4 is the same. We assumed that future nc-Si deposition will require only 25 and 13%, respectively, for the same thickness of the current SiH_4 and H_2 usages in a-Si deposition.

3.4. Module efficiency

We estimated the efficiency of the modeled PV modules under real operating conditions based on the performances of R&D modules. Commercial modules generally are less efficient than R&D modules mainly due to cost constraints and size effects, i.e., TCO performance, material quality, deposition uniformity, encapsulation loss, bus-bar shadow loss, wire loss, small shunts, and so on [11]. Therefore, cell efficiencies in the R&D stage must be translated cautiously into the rated efficiency of commercial modules. To estimate the efficiency of fully matured technology of the analyzed PV designs, we reviewed the efficiency records of those designs together with the current commercial module. The best one, the triple-junction a-Si/a-SiGe/a-SiGe is rated at total-area stabilized efficiency of 6.7% for United Solar's PVL-144, while PVL-136 analyzed in this study is rated at 6.3%, both with a module area of 2.16 m^2 [15]. The same type of cell rates at 13% for a small area of 0.25 cm^2 when combined with an Ag/ZnO back reflector and with a low deposition rate of 0.2 nm/s (Table III). Following this correlation (i.e., 6.3% versus 13%), we derived the real-world stabilized efficiency of the modeled designs of United Solar from the efficiencies measured under the R&D conditions by employing a factor of 0.48 (= 6.3/13). The reviewed literature regarding R&D cells of United solar indicates that, for triple-junction designs, a-Si/a-SiGe/nc-Si and a-Si/nc-Si/nc-Si perform at 13–13.3%, while, for tandem-junction configuration, a-Si/nc-Si remains at $\sim$12%. Accordingly, we suggest that the former designs will operate at the same stabilized efficiency, i.e., 6.3%, as the current commercial design, whereas the latter design will operate at around 5.8% ($= 0.48 \times 12\%$). We also added an efficiency scenario of 8%, benchmarking the current ''Micromorph'' technology that has a 7–9% stabilized efficiency for commercial modules [47,48].

Considering the added cost of energy and materials, the PV industry will not launch mass production of the listed new designs unless they are substantially more efficient than the current one. Herein, United Solar's near-term stabilized efficiency goal of 14% active-area efficiency, which corresponds to $\sim$7% for a large-area commercial module following the above estimate, may be the bottom line of future commercialization [39]. As discussed before, improved efficiency should be combined with a high rate deposition of nc-Si layer, i.e., 2–3 nm/s.

3.5. Other parameters

Other parameters, such as gas pressure and substrate temperature, were assumed to be the same as for a-Si deposition. Optimizing parameters is critical to boost deposition rate, and simultaneously obtain uniform quality over module area. The current triple-junction a-Si films are grown under a pressure of 0.1–1.3 mbar and temperatures of 150–300°C [49]. nc-Si layers normally are deposited

Table III. Stable efficiencies of a-Si/a-SiGe/a-SiGe triple-junction small (active) area and encapsulated large (aperture) area solar cells.

Source	Efficiency (%)	Dep. rate (nm/s)	Area (cm^2)	PECVD	Back reflector	Reference
Yang *et al.*, 1997	13.0	0.1	0.25	RF	Ag/ZnO	[62]
Banerjee *et al.*, 1999	10.5	0.1	920	RF	Ag/ZnO	[63]
Xu *et al.*, 2008	13.0	0.2	0.25	RF	Ag/ZnO	[36]
Yue *et al.*, 2008	10.2	0.6–0.8	0.25	VHF	Al/ZnO	[64]
Xu *et al.*, 2009	9.8	$\geq$0.6	464	VHF	Ag/ZnO	[65]

over a similar temperature range as a-Si [44,50–52]. On the other hand, nc-Si often is grown at a higher gas pressure, i.e., >2 mbar to escalate the deposition rate [51–54], although one study reports that the rate falls with a pressure over the range of 6–15 mbar [32]. These findings indicate that parameters often are machine-dependent and difficult to characterize. Controlling gas pressure at this small-scale may not significantly change the energy requirement during film deposition.

4. RESULTS

First, we compared the cradle-to-gate primary energy consumption for the commercial triple-junction a-Si with that of multi-junction a-Si modules with nc-Si as the bottom layer. A detailed energy analysis on the former is available elsewhere [21,35]. As Figure 5 shows, electricity consumption during film and contact deposition and module manufacturing are the primary sources of energy demand, followed by the encapsulation materials. The energy contribution from using the precursor gases varies from 1% for the current triple-junction system, to 5% for a-Si/nc-Si/nc-Si design as such usages are proportional to the total film's thickness. Among the current designs, a-Si/nc-Si/nc-Si exhibits the highest energy demand, reflecting the considerable thickness (3000–4500 nm) of the double nc-Si layers that are grown at a rate of 0.5–0.8 nm/s. An a-Si/nc-Si module requires a comparable amount of energy, ranging from 750 to 1270 MJ_p/m^2, as the current triple-junction module that requires 860 MJ_p/m^2. In contrast, the deposition of a-Si/a-SiGe/nc-Si and a-Si/nc-Si/nc-Si modules takes significantly more energy, ranging from 800–1390 and 950–1510 MJ_p/m^2, respectively (Figure 5(a)). The energy demands of these modules with nc-Si bottom layer, however, drop significantly in future scenarios to a level comparable to that of the current triple-junction a-Si (Figure 5(b)). The main underlying reason is the accelerated rate of nc-Si layer deposition, i.e., 2–3 nm/s, which lessens the duration of deposition for the same module.

We also compared, in Figure 6, the Energy Payback Times (EPBTs) of the PV module designs we considered. EPBT is defined as the period in years required for a renewable energy generation device to produce the same amount of energy as was invested to fabricating it (P). In measuring the period, both the energy produced by the device and the energy invested during device fabrication should be converted to a common form, usually to primary energy. We employed a primary energy-to-electricity conversion factor of 0.29, which represents the average

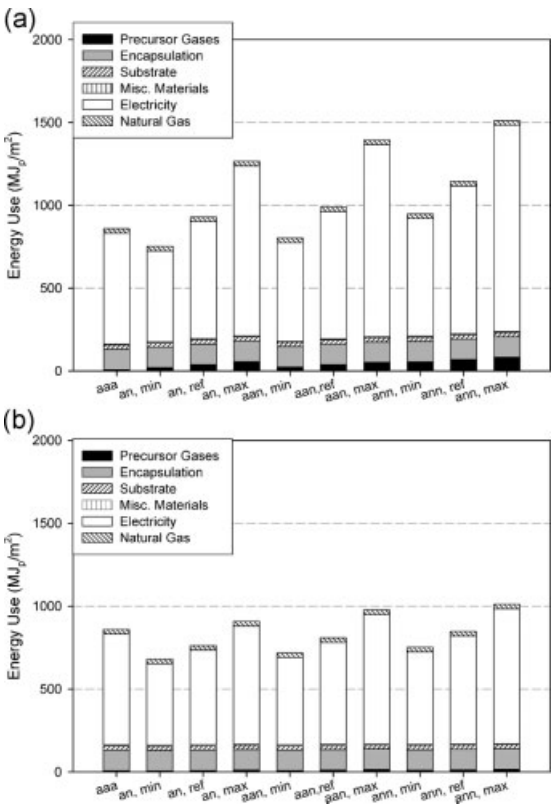

Figure 5. Cradle-to-gate usage of primary energy of the multi-junction combinations of a-Si and nc-Si: (a) current, and (b) future. ''aaa, an, aan, and ann'' respectively correspond to a-Si/a-SiGe/a-SiGe, a-Si/nc-Si, a-Si/a-SiGe/nc-Si, and a-Si/nc-Si/nc-Si. ''min'' scenario corresponds to the minimum thickness in Figure 1 with the fastest deposition rate in Table II while ''max'' scenario corresponds to the opposite. ''ref'' scenario employees the arithmetic means of the thickness and deposition rate for the two scenarios.

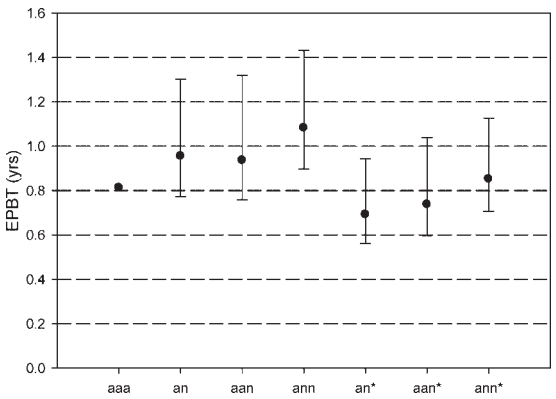

Figure 6. Energy payback time (EPBT) of the current multi-junction a-Si module options under average United States insolation, 1800 kWh/m^2/year, and a performance ratio of 0.75. ''aaa, an, aan, and ann,'' respectively, represent a-Si/a-SiGe/a-SiGe, a-Si/nc-Si, a-Si/a-SiGe/nc-Si, and a-Si/nc-Si/nc-Si. The estimated stabilized efficiency of the ''aaa'', ''aan'', and ''ann'' modules is 6.3%, while that of the ''an'' module is assumed as 5.8%. The designs with ''*'' are assumed to have a 8% efficiency. The high and low EPBTs correspond to the ''max'' and ''min'' cases for the production stage in Figure 5.

US grid mix, to convert the annual electricity generated by PV (A) to its primary energy equivalent. Thus, EPBT corresponds to A/P where A is a function of insolation (I), module efficiency (E), and performance ratio (R) (i.e., $A = I \times E \times R$). We used the US average insolation of 1800 kWh/m^2/year and a performance ratio of 0.75, which corresponds to a rooftop installation. Based on the efficiency records of the current R&D cells and the previously established ratio of 0.48, commercial production of a-Si/nc-Si modules are designated a stabilized efficiency of 5.8%, while that of a-Si/a-SiGe/nc-Si and a-Si/nc-Si/nc-Si are assumed to be 6.3%.

The EPBTs of the new designs, with nc-Si as a bottom layer for the reference cases, are significantly longer (i.e., 15–30%) than that of current triple-junction a-Si module, *viz.*, 0.8 years. EPBTs can be even longer for maximum impact scenarios (60–75%) which are based on the maximum thicknesses and slowest deposition rates. We readily explain this finding by the higher primary-energy requirement of the new design, illustrated in Figure 5(a). Moreover, the efficiencies of the new designs are not higher than that of the current triple junction. We note that our estimates of the EPBTs for the new designs are unrealistic as the alternatives, with such a low module efficiency, will not be commercialized. Therefore, we added scenarios with a more realistic efficiency, i.e., 8%, benchmarking the stabilized efficiency of commercialized ''Micromorph'' modules, 7.3–9.1% [47,48]. These scenarios, which with '*' in Figure 6, present the commercial bottom lines of energy payback times, i.e., 0.7–0.9 years. With an EPBT of < 1 year under the average US condition for the reference cases, all of these new designs exhibit potential advantages over bulk Si PVs whose EPBT is 1.2–1.7 years under the same condition [55]. Plotting in Figure 7 the EPBTs of the future scenarios with reduced primary-energy demand, given in Figure 5(b), against module efficiency reveals that future gains in module efficiency if coupled with a high rate of deposition and lower gas usages could reduce dramatically the EPBTs. For example, using the anticipated future efficiency of 10% for a-Si/nc-Si [56], the average EPBT corresponds to ~ 0.5 years for all designs.

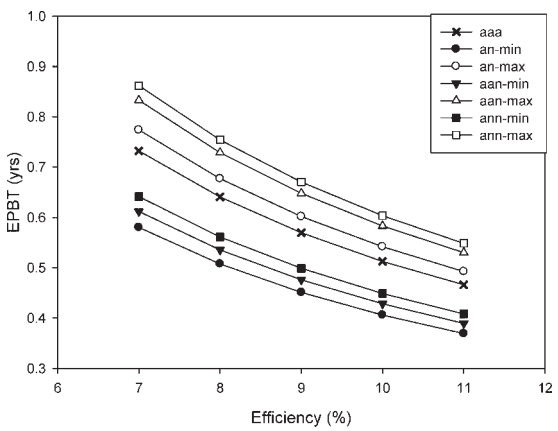

Figure 7. Energy payback time of future multi-junction a-Si module designs plotted over stabilized conversion efficiency under the average US insolation, 1800 kWh/m^2/year and a performance ratio of 0.75. ''aaa, an, aan, and ann'', respectively, correspond to a-Si/a-SiGe/a-SiGe, a-Si/nc-Si, a-Si/a-SiGe/nc-Si, and a-Si/nc-Si/nc-Si.

5. DISCUSSION

In our modeling, the PECVD energy requirement for a silicon film layer is proportional to the duration of deposition, and equivalently, to the thickness of film's layer. To examine the validity of this modeling, we compared the energy requirements we derived with that from similar processes in the semiconductor industry. Gutowski *et al.*'s review of manufacturing energy usage (2009) lists CVD processes, sorted by their materials-processing rate [57]. We converted their electricity values into primary energy terms by applying the US primary-to-electricity average conversion factor of 0.29 [58]. Figure 8 plots the PECVD energy-demands for a-Si and nc-Si films derived from the present modeling in parallel with Gutowski *et al.*'s data (2009) for semiconductor processing. According to their review, energy use declines with increasing materials-processing rate, as evidenced by the regression line. The materials-processing rates for a-Si and nc-Si films are the functions of deposition rate and gas inputs listed in Table II, and of the deposition area. The area of the current triple-junction a-Si module, 2.16 m^2, was employed to compute the gas-processing rate for a-Si and nc-Si layers. The materials-processing rate for current nc-Si deposition is higher than that for a-Si deposition because the former is assumed to use twice the amount of H_2 than the latter, and also to employ a higher rate of deposition (i.e., 0.5–0.8 nm/s versus 0.1–0.3 nm/s). The energy demand during a-Si deposition, normalized per kg of precursor gases, is consistent with information on SiO_2/Si_3N_4 deposition reported by the semiconductor industry

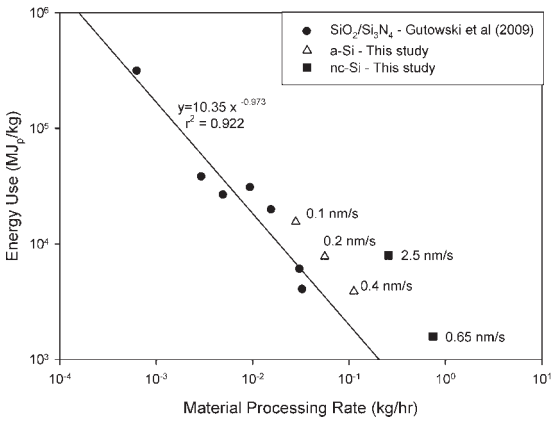

Figure 8. Energy use of chemical vapor deposition (CVD) processes versus precursor gas processing rate [57].

[57], validating our energy modeling. However, the energy usages per kg of gases during nc-Si deposition from our modeling diverge from the estimated trend because of its higher materials-processing rate than a-Si deposition. Notably, estimated energy usage per kg of gases for future nc-Si deposition is much higher than that for current deposition due to the assumed higher gas utilization (i.e., 80 versus 20%). In other words, less gas is needed for depositing the same thickness of layers in future nc-Si deposition, *viz*., higher energy use per kg of gas usage. This indicates that our model of the future nc-Si deposition rests on a different mechanism than the current processing. Further discussion of this high-rate, high gas-utilization deposition technique is beyond this study's scope.

The main obstacles against increasing the deposition rate of nc-Si for a large module are the issues of film quality and uniformity that affect module efficiency [11]. A fundamental question is whether deposition rates can be raised without significantly sacrificing the conversion efficiency. Saito *et al*. (2005) shows that this can be achieved at least for a-Si/nc-Si/nc-Si type of design [32]. Deposition techniques other than RF and VHF PECVD aim to boost the deposition rate of nc-Si, such as hot-wire chemical vapor deposition (HWCVD) wherein the electrode is replaced with heated filament of 1800–2000°C generating ions and radicals. HWCVD can deposit layers at a rate of up to 30 nm/s under R&D conditions, although a large-scale operation has yet to be demonstrated due to poor film quality and uniformity [11]. Apparently, the implications of this technology on life-cycle energy usage will differ from the RF and VHF PECVD analyzed here, so warranting further analysis.

A similar version of the a-Si/nc-Si PV analyzed in this study, the ''Micromorph'' tandem design has already been commercialized based on a different encapsulation and contact layer configuration. The commercialized Micromorph design employs double-glass, each ~ 3 mm thick, compared to the ~ 0.1 mm stainless steel substrate in the analyzed designs (Figure 9). It also includes textured zinc oxide contact layer with a thickness of $\sim 2\,\mu$m, which is deposited by the low pressure chemical vapor deposition (LPCVD) process, while the analyzed a-Si/nc-Si design uses flat, 70 nm ITO contact. The current stabilized module efficiency for the Micromorph design is 7–9% [47,48]. We estimated the energy imbedded in this design based on the material composition and layer configuration. First, we use the imbedded energy of encapsulation in the thin-film CdTe module that has a similar configuration as the Micromorph design i.e., double-glass with polymer lamination. This corresponds to 330 MJ_p/m^2 compared to 150 MJ_p/m^2 in the encapsulation of analyzed a-Si/nc-Si, i.e., stainless steel substrate with EVA. Then, for the zinc oxide contact, since the energy required for LPCVD is unavailable, we assume the same amount of energy per thickness as the PECVD uses to grow a-Si layers. Finally, assuming other parameters including the thicknesses of Si layers and back reflector being the same as the analyzed a-Si/nc-Si, we estimate a primary energy demand of 1300 MJ_p/m^2 for the Micromorph design. This corresponds to a $\sim$40 % increase from the energy to manufacture the analyzed a-Si/nc-Si design, i.e., 930 MJ_p/m^2 (Figure 5(a)). Yet, with a stabilized module efficiency of 9%, the Micromorph design's energy payback time is 0.9 years, close to those for the analyzed multi-junction designs with 8% efficiency, 0.7–0.9 years (Figure 6). We note that there exists a large degree of uncertainty in this estimate as the manufacturing process used for the Micromorph design is different from that used for the analyzed a-Si/nc-Si. Unlike roll-to-roll deposition used in United Solar, the batch PECVD cycle used for the Micromorph design entails loading and unloading the substrate for each layer deposition. Moreover, the reactor is cleaned by SF_6 or NF_3 between deposition of every layer to avoid contamination. Processing energy demand, encapsulation materials and cleaning gases need to be inventoried in further detail for an accurate energy estimate, which remains as a future topic of investigation.

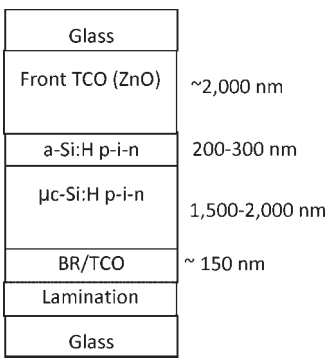

Figure 9. Configuration of micromorph a-Si PV [27,60,61].

6. CONCLUSIONS

While multi-junction a-Si PV modules with a nanocrystalline-silicon bottom layer have demonstrated great potential for increasing the efficiency of photon-to-electricity conversion, the life-cycle energy and environmental implication of such designs has yet to be investigated. In this study, we proactively measured the environmental performance, i.e., energy payback time (EPBT), of this immature technology based on current R&D findings and the projected parameters of PECVD, the film-deposition technology using United Solar's module configuration. We also parametrically evaluate the energy implication of a commercial version of this type, Micromorph. Our study suggests that inserting nc-Si layers in multi-junction a-Si PVs may significantly raise the embedded energy per unit area, primarily because of the prolonged deposition time and increased use of precursor gases. Therefore, boosting the deposition rate of nc-Si layers is crucial from both economic and environmental perspective. Increased deposition rates must be accompanied by a substantial

increase in module efficiency before they are commercialized. If the current R&D processing is scaled-up, the EPBT of the multi-junction modules with nc-Si layers will increase from 0.8 to 0.9–1.1 years in the reference case. A more realistic scenario assuming a higher product efficiency (8%) indicates that the EPBT will be 0.7–0.9 years, suggesting the potential energy benefits of this type upon commercialization. Projected future technologies could complete nc-Si deposition around four times faster. According to future scenarios with a projected efficiency of 10% and deposition rate of 2–3 nm/s, the EPBTs could further drop by $\sim$30% from the above scenario. Besides PECVD, other film-deposition technologies might produce nc-Si at an even higher rate, although the deposition quality is not satisfactory yet. A timely update of this analysis will be needed in the future if these new technologies dominate.

ACKNOWLEDGEMENTS

We are grateful to Dr Subhendu Guha, United Solar, for data provided and his review of the paper, and to Dr Sergio Pacca at University of São Paulo for providing details of his previous work. This research is supported from the EPA STAR program under grant # RD-8333340 to CU (HCK), and from the USDOE Contract DE-AC02-76CH000016 to BNL (VMF).

REFERENCES

1. Khanna V, Bakshi BR. Carbon nanofiber polymer composites: evaluation of life cycle energy use. *Environmental Science and Technology* 2009; **43**(6): 2078–2084.
2. Khanna V, Bakshi BR, Lee LJ. Carbon nanofiber production: life cycle energy consumption and environmental impact. *Journal of Industrial Ecology* 2008; **12**(3): 394–410.
3. Krishnan N, Boyd S, Somani A, Raoux S, Clark D, Dornfeld D. A hybrid life cycle inventory of nano-scale semiconductor manufacturing. *Environmental Science and Technology* 2008; **42**(8): 3069–3075.
4. Lloyd SM, lave LB. Life cycle economic and environmental implications of using nanocomposites in automobiles. *Environmental Science and Technology* 2003; **37**(15): 3458–3466.
5. Lloyd SM, Lave LB, Matthews HS. Life cycle benefits of using nanotechnology to stabilize platinum-group metal particles in automotive catalysts. *Environmental Science and Technology* 2005; **39**(5): 1384–1392.
6. Meyer DE, Curran MA, Gonzalez MA. An examination of existing data for the industrial manufacture and use of nanocomponents and their role in the life cycle impact of nanoproducts. *Environmental Science and Technology* 2009; **43**(5): 1256–1263.
7. Osterwalder N, Capello C, Hungerbűhler K, Stark WJ. Energy consumption during nanoparticle production: how economic is dry synthesis? *Journal of Nanoparticle Research* 2006; **8**: 1–9.
8. Roes AL, Marsili E, Nieuwlaar E, Patel MK. Environmental and cost assessment of a polypropylene nanocomposite. *Journal of Polymers and the Environment* 2007; **15**: 212–226.
9. Bauer C, Buchgeister J, Hischier R, Poganietz WR, Schebek L, Warsen J. Towards a framework for life cycle thinking in the assessment of nanotechnology. *Journal of Cleaner Production* 2008; **16**: 910–926.
10. Guzman KAD, Taylor MR, Banfield JF. Environmental risks of nanotechnology: national nanotechnology initiative funding, 2000–2004. *Environmental Science and Technology* 2006; **40**: 1401–1407.
11. Deng X, Schiff EA. Amorphous silicon–based solar cells. In Luque A, Hegedus S (eds). Handbook of Photovoltaic Science and Engineering. John Wiley & Sons: West Sussex, UK, 2003.
12. Wronski CR, Carlson DE. Amorphous silicon solar cells. In Archer MD, Hill R (eds). Clean Electricity from Photovoltaics. Imperial College Press: London, UK, 2001.
13. Green MA, Emery K, Hishikawa Y, Warta W. Solar cell efficiency tables (Version 34). *Progress in Photovoltaics: Research And Applications* 2009; **17**: 320–326.
14. Hegedus S. Thin film solar modules: the low cost, high throughput and versatile alternative to Si wafers. *Progress in Photovoltaics: Research and Applications* 2006; **14**: 393–411.
15. United Solar Ovonic. Standard Products Technical Data Sheets, 2009.
16. Grama S, Bradford T. Thin-Film PV 2.0: Market Outlook Through 2012. The Prometheus Institute, 2008.
17. Nozik AJ. Quantum Dot Solar Cells. National Renewable Energy Laboratory: Golden, CO, 2001.
18. Alsema E. Energy requirements of thin-film solar cell modules-a review. *Renewable & Sustainable Energy Reviews* 1998; **2**: 387–415.
19. Keoleian GA, Lewis GM. Application of life-cycle energy analysis to photovoltaic module design. *Progress in Photovoltaics: Research and Applications* 1997; **5**: 287–300.
20. Keoleian GA, Lewis GM. Modeling the life cycle energy and environmental performance of amorphous silicon BIPV roofing in the US. *Renewable Energy* 2003; **28**: 271–293.
21. Pacca S, Sivaraman D, Keoleian GA. Parameters affecting the life cycle performance of PV technologies and systems. *Energy Policy* 2007; **35**: 3316–3326.
22. Fthenakis V, Gualtero S, van der Meulen R, Kim HC. Environmental implications of nanostructured photovoltaics: a comparative life-cycle analysis framework. *Materials Research Society Symposium Proceeding, 1041-R01-04*, 2007.

23. Staebler DL, Wronski CR. Reversible conductivity changes in discharge-produced amorphous Si. *Applied Physics Letters* 1977; **31**(4): 292.
24. Guha S. Multijunction solar cells and modules. In Street RA (ed.). Technology and Applications of Amorphous Silicon. Springer: 2000.
25. Wronski CR, Roedern BV, Kołodziej A. Thin-film Si:H-based solar cells. *Vacuum* 2008; **82**: 1145–1150.
26. Wronski CR, Collins RW. Phase engineering of a-Si:H solar cells for optimized performance. *Solar Energy* 2004; **77**: 877–885.
27. Shah A, Meier J, Buechel A, Kroll U, Steinhauser J, Meillaud F, Schade H, Dominé D. Towards very low-cost mass production of thin-film silicon photovoltaic (PV) solar modules on glass. *Thin Solid Films* 2006; **502**: 292–299.
28. Vetterl O, Finger F, Carius R, Hapke P, Houben L, Kluth O, Lambertz A, Mück A, Rech B, Wagner H. Intrinsic microcrystalline silicon: a new material for photovoltaics. *Solar Energy Materials & Solar Cells* 2000; **62**: 97–108.
29. Meier J, Kroll U, Benagli S, Roschek T, Huegli A, Spitznagel J, Kluth O, Borello D, Mohr M, Zimin D, Monteduro G, Springer J, Ellert C, Androutsopoulos G, Buechel G, Zindel A, Baumgartner F, Koch-Ospelt D. Recent progress in up-scaling of amorphous and micromorph thin film silicon solar cells to 1.4 m2 modules. *Materials Research Society Symposium Proceeding, 0989-A24-01*, 2007.
30. Smets AHM, Matsui T, Kondo M. High-rate deposition of microcrystalline silicon p-i-n solar cells in the high pressure depletion regime. *Journal of Applied Physics* 2008; **104**: 034508.
31. Life cycle Analysis of CdTe Photovoltaic Systems, Including Alternative Cd use and Disposal Scenarios in the EU, *Progress Report*. Brookhaven National Laboratory, Upton, NY, 2009.
32. Saito K, Sano M, Okabe S, Sugiyama S, Ogawa K. Microcrystalline silicon solar cells fabricated by VHF plasma CVD method. *Solar Energy Materials & Solar Cells* 2005; **86**: 565–575.
33. Alsema E, Fraile D, Frischknecht R, Fthenakis V, Held M, Kim HC, Pölz W, Raugei M, de Wild Scholten M. *Methodology Guidelines on Life Cycle Assessment of Photovoltaic Electricity, Subtask 20 ''LCA''*, International Energy Agency PVPS Task 12, 2009.
34. Izu M, Ellison T. Roll-to-roll manufacturing of amorphous silicon alloy solar cells with *in situ* cell performance diagnostics. *Solar Energy Materials & Solar Cells* 2003; **78**: 613–626.
35. Pacca S, Sivaraman D, Keoleian GA. Life cycle assessment of the 33 kw photovoltaic system on the dana building at the university of michigan: thin film laminates, multi-crystalline modules, and balance of system components. Center for Sustainable Systems, University of Michigan: Ann Arbor, MI, 2005.
36. Xu X, Yan B, Beglau D, Li Y, DeMaggio G, Yue G, Banerjee A, Yang J, Guha S, Hugger PG, Cohen JD. Study of large area a-Si:H and nc-Si:H based multi-junction solar cells and materials. *Materials Research Society Symposium Proceeding, 1066-A14-02*, 2008.
37. Hinson S, Ranum D, Haung T. Analysis of energy usage in three process tools. International SEMATECH, 2000.
38. Huang T. Strategies for energy reduction in semiconductor manufacturing. *SolidState Technology* 2008; (October): 30–35.
39. Yan B, Yue G, Guha S. Status of nc-Si:H solar cells at united solar and roadmap for manufacturing a-Si:H and nc-Si:H based solar panels. *Materials Research Society Symposium Proceeding, Vol. 989, 0989-A15-01*, 2007.
40. Matsui T, Matsuda A, Kondo M. High-rate microcrystalline silicon deposition for p-i-n junction solar cells. *Solar Energy Materials & Solar Cells* 2006; **90**: 3199–3204.
41. Hamers EAG, van den Donker MN, Stannowski B, Schlatmann R, Jongerden GJ. Helianthos: roll-to-roll deposition of flexible solar cell modules. *Plasma Processes and Polymers* 2007; **4**: 275–281.
42. Yue G, Yan B, Yang J, Guha S. High rate deposition of amorphous silicon based solar cells using modified very high frequency glow discharge. *Materials Research Society Symposium Proceeding, 0989-A15-04*, 2007.
43. Kroll U, Meier J, Torres P, Pohl J, Shah A. From amorphous to microcrystalline silicon films prepared by hydrogen dilution using the VHF (70 MHz) GD technique. *Journal of Non-crystalline Solids* 1998; **227**: 68–72.
44. Strahm B, Howling AA, Sansonnens L, Hollenstein C. Plasma silane concentration as a determining factor for the transition from amorphous to microcrystalline silicon in SiH_4/H_2 discharges. *Plasma Sources Science and Technology* 2007; **16**: 80–89.
45. Guha S, Yang J. High-efficiency amorphous silicon alloy based solar cells and modules. National Renewable Energy Laboratory, 2005.
46. Kluge MD, Ray JR. Amorphous-silicon formation by rapid quenching: a molecular-dynamics study. *Physical Review B* 1987; **36**(8): 4234–4237.
47. *Kaneka introduces a newly developed Hybrid PV module to the US market and opens a US Office in Texas*, 2009. Press release, December 1. http://www.pv.kaneka.co.jp/press_release/091201.html
48. Datasheet:X-Series-MICROMORPH. Inventux Technology AG, 2009.
49. Guha S, Yang J, Banerjee A. Amorphous silicon alloy photovoltaic research—present and future. *Progress in Photovoltaics: Research and Applications* 2000; **8**: 141–150.
50. Keppner H, Meier J, Torres P, Fischer D, Shah A. Microcrystalline silicon and micromorph tandem solar cells. *Applied Physics A: Materials Science & Processing* 1999; **69**: 169–177.

51. Matsui T, Matsuda A, Kondo M. High-rate plasma process for microcrystalline silicon: over 9% efficiency single junction solar cells. *Materials Research Society Symposium Proceeding, 808-A8.1.1*, 2004.
52. Gordijn A, Francke J, Hodakova L, Rath JK, Schropp REI. Influence of pressure and plasma potential on high growth rate microcrystalline silicon grown by VHF PECVD. *Materials Research Society Symposium Proceeding, Vol. 862 A10.3.1*, 2005.
53. Rech B, Roschek T, Müller J, Wieder S, Wagner H. Amorphous and microcrystalline silicon solar cells prepared at high deposition rates using RF (13.56 MHz) plasma excitation frequencies. *Solar Energy Materials & Solar Cells* 2001; **66**: 267–273.
54. Strahm B, Howling AA, Sansonnens L, Hollenstein C. Optimization of the microcrystalline silicon deposition efficiency. *The Journal of Vacuum Science and Technology A* 2007; **25**(4): 1198–1202.
55. Fthenakis V, Kim HC, Held M, Raugei M, Krones J. Update of PV energy payback times and life-cycle greenhouse gas emissions. *24th European Photovoltaic Solar Energy Conference*, Hamburg, Germany, 2009.
56. von Roedern B, Ullal HS. The role of polycrystalline thin-film PV technologies in competitive PV module markets. *33rd IEEE Photovoltaic Specialists Conference*, San Diego, CA, 2008.
57. Gutowski TG, Branham MS, Dahmus JB, Jones AJ, Thiriez A, Sekulic DP. Thermodynamic analysis of resources used in manufacturing processes. *Environmental Science & Technology* 2009, **43**: 1584–1590.
58. Franklin Association US LCI Database Documentation: Prairie Village, KS, USA, 1998.
59. Pacca S. Personal communication, 2006.
60. Oerlikon. *Solar extends its lead in thin film silicon technology with new TCO 1200 plant*, 2007. Press release, June 21. http://www.oerlikon.com/ecomaXL/index.php?site=OERLIKON_EN_archive_2007_detail&udtx_id=4292
61. Söderström T, Haug F-J, Niquille X, Ballif C. TCOs for nip thin film silicon solar cells. *Progress in Photovoltaics: Research and Applications* 2009; **17**: 165–176.
62. Yang J, Banerjee A, Guha S. Tripje-junction amorphous silicon alloy solar cell with 14.6% initial and 13.0% stable conversion efficiencies. *Applied Physics Letters* 1997; **70**(22). 2975–2977.
63. Banerjee A, Yang J, Guha S. Optimization of high efficiency amorphous silicon alloy based triple-junction modules. *Materials Research Society Symposium Proceeding, Vol. 557 1999: 743*.
64. Yue G, Yan B, Yang J, Guha S. Hydrogenated amorphous silicon and silicon germanium triple-junction solar cells at high rate using RF and VHF glow discharges. *33rd IEEE Photovoltaic Specialists Conference*, San Diego, CA, 2008.
65. Xu X, Beglau D, Ehlert S, Li Y, Su T, Yue G, Yan B, Lord K, Banerjee A, Yang J, Guha S, Hugger PG, Cohen JD. High efficiency large area a-Si:H and a-SiGe:H multi-junction solar cells using MVHF at high deposition rate. *Materials Research Society Symposium Proceeding,1153-A07-01*, 2009.